KAPL-P-000008
(K95069)

ANALYSIS OF WARM PRESTRESS DATA

B. D. Macdonald, G.T. Embley, H. Irizarry-Quinones, W. J. McAfee, D. E. McCabe,
P. D. Smith, J. W. Wuthrich

June 1995

NOTICE

KAPL ATOMIC POWER LABORATORY SCHENECTADY, NEW YORK 12301

Operated for the U. S. Department of Energy
by KAPL, Inc. a Lockheed Martin company

DISCLAIMER

Analysis of Warm Prestress Data

BD Macdonald[1], GT Embley[1], H. Irizarry-Quinones[1],
WJ McAfee[2], DE McCabe[2], PD Smith[1], and JW Wuthrich[1]

Abstract

Loading a cracked structure at elevated temperature, or warm prestressing (WPS), enhances its fracture resistance at a lower temperature. Five data sets, comprising 119 unclad pressure vessel steel specimens, were combined to derive correlations for WPS-enhanced fracture toughness (K_{Ifrac}) in the absence of ductile tearing. New WPS test results for 27 surface flawed specimens, eight subclad flawed specimens, and five strain-aged specimens are discussed. K_{Ifrac} exceeded non-WPS fracture toughness, K_{Ic}, for all experiments. The WPS data showed that no specimens failed while K was decreasing, and that at least an additional seven percent additional reloading from the minimum value of applied K_I took place prior to final fracture. The data included complete and partial unloading after WPS prior to final fracture. Crack tip 3-dimensional elastic-plastic finite element (3DEPFE) analysis was performed to support statistical analysis of the data. Regression models were compared with the Chell WPS model.

Crack tip 3DEPFE analysis indicated that partially unloaded and completely unloaded data should be treated separately, and that the amount of unloading is unimportant for partially unloaded data.The regression models, which use K_I at WPS (K_{Iwps}) and K_{Ic} as independent variables, better represented the WPS benefit than did the more complicated Chell model. An adequate accounting was made for constraint in the WPS experiments. The subclad flaw data support the use of the partial unload regression model, provided that some care is taken to represent the effect of intact cladding if present. The effect of strain aging at or below 260 C (500 F) on WPS benefit was of no consequence for the pressure vessel steels and WPS temperatures used to derive the regression models. The presence of ductile tearing precludes the use of the regression models. The regression model for partial unloading accurately predicted the behavior of full scale pressure vessel WPS experiments. All but one of the 174 experiments considered lie above the lower 2σ estimate of the regressions. The experiments all supported Type I WPS, i.e., There was no fracture during cooling until reloading occurred. However, the regression equations apply to the reload, and are inapplicable to Type I WPS.

Introduction

If a flaw is stressed at elevated temperature, and then loaded to fracture at a lower temperature, the apparent fracture toughness will be higher than it would be if no prestressing at the elevated temperature had taken place. This is called the warm prestressing (WPS) effect. Experiments on pressure vessel steels suggest that the enhancement of fracture toughness at lower temperatures is due to the development of a plastic zone surrounding the border of the flaw at higher temperatures which is locked in place due to elevation of strength at lower temperatures. Various continuum mechanics models describing WPS benefit have been proposed. The applicability of these models depends on the availability and accuracy of input information derived from the application of other thermal, continuum, and material behavior models, all of which are sources of error. It is therefore prudent to simplify the WPS model to reduce the chance of error during its application. The objective of this analysis was to quantify WPS benefit with an empirical model that was as simple and accurate as possible. The resulting model was based on statistical analysis of the data supported by finite element analysis of the crack tip during unloading.

[1] Knolls Atomic Power Laboratory, Box 1072, Schenectady, NY 12301-1072
[2] Oak Ridge National Laboratory, Oak Ridge, TN 37831-8056

Previous Work, Materials, Specimen Geometry, and Load Paths

The data included in this study, Table 1, were from A508-Class 2 and A533-B pressure vessel steels in various specimen configurations, and subjected to a wide variety of load paths believed to span most practical applications. The data included unloading after WPS of anywhere between 0% and 100% of the WPS load prior to final fracture. The KAPL/ORNL clad and unclad surface cracked beam, PS(B), specimens are discussed in Appendix A. Analysis showed that K was nearly constant along the crack front for these specimens. Loss et al tested single edge bend, SE(B), specimens in two thicknesses (Loss 1977). Andrews tested shallow cracked SE(B) specimens heat treated to several strength levels (Andrews 1970). Chell et al tested middle cracked tension, M(T), specimens in two strength levels (Chell 1980). Stonesifer et al tested 202mm thick compact tension,4TC(T), specimens (Stonesifer 1989).

Lidbury and Birkett's report (Lidbury 1988) did not include the necessary data to either verify their calculations or make other use of their test results. The same is true of the reports by Succop et al (Succop 1970), Nichols (Nichols 1968), Pokrovsky et al (Pokrovsky 1994), and Haigh (Haigh 1984). Shum's report (Shum 1993) deals with the possibility of interpreting WPS as a fracture mechanics constraint issue, but provides no test data. Hollstein et al (Hollstein 1986), Curry (Curry 1981) and Okamura et al (Okamura 1994) presented graphical data which was scaled and plotted for comparison with the models derived in the present work. These data were not included in the database due to expected scaling inaccuracies.

All told, 119 unclad WPS experiments were included in the database used to define the regression models for comparison with the Chell model. This data base includes no specimens for which ductile tearing occurred either during WPS, or after unloading, prior to final fracture. No specimens failed while K was decreasing. At least 9% additional reloading from the minimum value of applied K_I occurred before fracture. Strain aged, subclad flaw, and ductile tearing WPS data were compared with the regression model results.

Interpretation of Fracture Resistance

The virtual crack extension method (de Lorenzi 1982) used for calculating the J-integral for the elastic-plastic surface flaw specimens (KAPL / ORNL data) depends upon the applicability of deformation theory of plasticity to the state of stress. Therefore, the path-dependent unloading and reloading to fracture which occurs in the WPS evolution could not be addressed with this approach. Since the strip yield model was not considered appropriate for the surface flaw data, the following interpretation of the final fracture resistance was used. For each WPS fracture toughness specimen, the load at fracture was considered to have characterized the influence of WPS, unloading, and reloading to fracture on the region surrounding the pre-existing crack. In order to compare correlation results for the various types of specimens, the enhanced post-WPS fracture toughness, K_{Ifrac}, was determined in the following manner. The load at fracture was multiplied by the elastic plane strain geometry constant required to form the elastic stress intensity factor at fracture, as shown for example on Figure 3. This value was amplified by the plane strain plastic zone correction factor to form K_{Ifrac}. This interpretation was perhaps simplistic, but no more complicated procedure was thought to be any more applicable. A similar approach was taken to determine K_{Iwps}. During WPS loading of KAPL/ORNL specimens, considered to have the lowest constraint of all examined, K_{Iwps} was at most 10.5% lower than K(J) at the WPS load. This suggests that the plastic zone corrected stress intensity factor was adequate to the task of interpreting the WPS data.

Constraint Effects

Loss of triaxial tension (constraint) along the crack front has been shown by many investigators to enhance the apparent material fracture toughness compared to its plane strain value (Reuter 1987). This effect was neutralized in the WPS experiments as follows. In the analysis of the WPS specimens, K_{Ifrac} was found to vary directly with the non-WPS fracture toughness at final fracture temperature as determined from control specimens which were of the same geometry as the WPS specimens. Clearly, the load at fracture of the KAPL/ORNL. Chell, and Andrews specimens was influenced by the loss of constraint due to the proximity of free surfaces to the crack front. However, the constraint effect was compensated for because it was the same in both the WPS and control specimens. If this matched constraint approach had not been taken, the impact on data correlations would have been significant. For example, consider the KPAL/ORNL PS(B)specimens. K_I at fracture for the control specimens was twice the K_{Ic} value obtained from compact tension specimens, as was the case in a previous investigation (Reuter 1987). Hence, WPS models dependent upon this value would give vastly different results if K_{Ic} were used rather than the control specimen value of K_I at fracture. On the other hand, application of the resulting WPS models to hypothetical surface flaws would be conservative. This is because K_{Ic} rather than the control specimen value of K_I at fracture would be used to predict the WPS-enhanced fracture toughness which varies directly with K_{Ic}. Further justification for this approach will be found in what follows, by noting that the regressions are applicable to both relatively low and high constraint data.

Data Analysis and Predictive Models

Two approaches for estimating WPS fracture toughness were compared. The first was due to Chell (Chell 1980) which is based on Dugdale's strip-yielding model. It predicts a value of WPS enhanced fracture toughness, K_I-Chell, which depends upon K_{Iwps}, K_I minimum at unload, K_{Ic} at fracture temperature, and flow stress at the temperatures associated with WPS, minimum load, and fracture. The second approach was to derive empirical, linear regression models which predict a value of WPS enhanced fracture toughness dependent upon K_{Iwps} and K_{Ic} at fracture temperature. This choice of independent variables was supported by a statistical analysis of variance (ANOVA) as discussed below. The ANOVA showed that WPS benefit was not a strong function of amount of unloading. Chell and Haigh (Chell 1986) had also proposed a less complex model in which K_{Ifrac} depended upon K_{Iwps}, K_{Ic}, and percent unloading prior to fracture. Although this model was not considered in the present study, the ANOVA implied that even this simplified model may be more complex than is necessary. The accuracies of the original Chell model and the linear regression models were compared on the basis of their ability to minimize the K_{Ifrac} scatter for the data sets included in this study. For the reasons stated above, in what follows, K_{Ic} refers to the control specimen value of K_I at fracture even though valid K_{Ic} values were only obtained for the Loss et al and Stonesifer et al control specimens.

The small scale yielding equations for the Chell model (Chell 1980) were applied to the five data sets. Six specimens from the Chell data set (Chell 1980) were excluded due to the presence of excessive plasticity. The data used in this study are presented in Table 1.

Chell Model Results

K_{Ifrac} is plotted vs K_I-Chell in Figure 1a for all the data of Table 1, regardless of the amount of unloading occurring after WPS and prior to fracture. The correlation coefficient (R^2), and

standard error (SE or σ) are shown in Table 2. Also shown are the R^2 and SE for separate analyses for K_I-Chell of complete (100%) unloading and partial (0-80%) unloading for comparison with the regression analyses.There is no remarkable change in either R^2 or SE when the data are separated into these groups.

Statistical Analysis of Test Results

A model with seven independent variables was investigated first, using all of the data, regardless of the amount of unloading. Later, similar analyses were performed on the 100% unload data, and on the 0-80% unload data treated separately. The seven term model had three continuous main effects (K_{Iwps}, Kmin, and fracture temperature) and their first interactions, as well as the load path. To better compare the separate data sources, the fracture temperature was replaced with the material (control) K_{Ic} value. An ANOVA was performed and the significance of each term in the model was examined. The term with the lowest significance was removed and the model was re-analyzed. The statistical significance of the change in the model was then evaluated. Errors were also calculated to insure that the overall change to the error term remained insignificant. This process was repeated until the results showed that no additional terms could be removed from the model at the 95% confidence level.

When all the data were combined, only the load path could be removed. If a smaller risk were assumed, then the model could be reduced to the primary effects only. However, this model may be undesirable because Kmin may not be well defined in practice. Figure 1b shows the Measured vs. Predicted plot for the model with K_{Iwps}, Kmin, and K_{Ic} and their first interactions. Only one KAPL/ORNL data point was seen to be greater than 3 standard errors from the predicted values. The correlation, correlation coefficient (R^2), and standard error (SE) are shown in Table 2.

Since the occurrence of 100% unloading is unlikely in practice, the 100% unloading data and 0-80% unloading data were separated from each other. The reduction of the full seven term starting model was performed for each data set. The reduction for the 100% unloading data yielded a regression in terms of K_{Iwps} and K_{Ic} shown in Table 2 and Figure 2. For the partial unload data, the K_{Iwps}*K_{Ic} and loading path variables remained along with K_{Iwps} and K_{Ic}. However, analysis of the model with the K_{Iwps}*K_{Ic} and loading path terms removed showed the effect caused by their removal was small. This further reduction was considered justified since the loading path will in practice be poorly defined. The removal of these terms caused a negligible reduction in the R^2 term (0.958 to 0.945) and only a small increase in the standard error (7.90 to 8.79). The correlation, R^2, and SE are shown in Table 2 and the data in Figure 2.

Comparison of WPS Models

Table 2 shows that some improvement in R^2 and SE was attained with the regression models compared to Chell's model. This was expected, since the regression is based on test results, while the Chell model is a fracture mechanics idealization that was derived independently of any test results. Separation of the regression models into partial (0-80%) and complete (100%) unloading after WPS and prior to fracture led to a significant model simplification compared to inclusion of all the data. Also, the amount of unloading was not found to be important for the partial unloading data. This suggests that the simplified Chell model (Chell 1986) may still be more complex than is necessary. Additional support for these conclusions was sought through a description of the crack tip stress field, as discussed next.

Crack Tip Opening Stress During Unloading

Far field observations, such as load-displacement records, were not expected to provide any insight, since the WPS phenomenon is highly localized at the crack tip. Therefore, 3-dimensional elastic-plastic finite element (3DEPFE) analysis results for surface flawed specimens were examined. The study was restricted to the results at the maximum depth of the flaw in order to gain some insight for through-cracked specimens, as well.

Kinematic strain hardening was assumed for the incremental plasticity analysis of the finite element model. Crack opening stress, σ_{yy}, was determined at the Gauss point closest to the crack tip and nearest to the plane of expected crack extension. This Gauss point was about 0.022mm (0.875E-03 in) distant from the crack tip. A similar calculation was repeated for comparable Gauss points in each of the elements surrounding the crack tip at maximum crack depth. These stresses were determined at the WPS load and several unloading values, including 100% unload.

The σ_{yy} stress is plotted as a function of theta, measured from the plane of crack extension as shown in Figure 3. The variation of σ_{yy} with theta is fairly insensitive to the amount of unloading. The region ahead of the crack (theta = 0°) becomes compressed about the same amount regardless of the amount of unloading. This supports the statistical analysis result that the amount of unloading is not important. It is further noted that the crack flank (theta = 180°) becomes compressed only at complete unloading. This response may influence the 100% unloading data differently upon reloading than the partial unload data. This observation appears to support separation of the 100% unloading data from the rest.

Analysis of Subclad Flaw WPS Beams

Eight clad beam WPS specimens, tested as described in Appendix A, were considered to be results of structural flaw tests, and were intended for comparison with the regression model generated from the more numerous unclad data. Test results are presented in Table 3. Nominal amounts of unloading for the clad beams were 33% and 67%. Therefore, in what follows, the partial unload regression model is regarded as the basis for a behavior prediction with which the clad data were compared (for conservatism).

Three dimensional, elastic-plastic, finite element (3DEPFE) J-integral analysis of the clad beams was used to estimate the value of K_{Ifrac} for the clad WPS specimens, because the presence of yielded cladding precluded use of the elastic K solution for the surface flaw. This analysis was also used to estimate K_{Iwps} from the WPS load for use in the regression equation. As was the case with the unclad beams, the unclad non-WPS beam fracture toughness data were used to estimate K_{Ic} for use in the regression equation. This approach leads to K_{Ifrac} values which scattered within and above the partial unload data, Figure 4, the large bold "X" symbol. Next the Kaya-Erdogan solution for an edge loaded edge crack (Kaya 1980) was used to represent the effect of cladding, assuming the cladding to act uniformly in tension at its yield stress. The subclad flaw data are again plotted in Figure 4, the large regular "X" symbol, using plastic zone corrected K calculations for the model, and the J-integral based value of K_{Ifrac} of Figure 4. These data support the use of the partial unload regression model for subclad flaws, provided that some care is taken to represent the effect of intact cladding if present.

Strain Aging Effects

Increased strength and loss of ductility may occur if yielded material is exposed to elevated temperature for some period of time, resulting in strain aging. It is caused by the diffusion of carbon and nitrogen to dislocations, which results in their being repinned (Dieter 1961). Subjecting the crack front plastic zone (which was yielded due to a WPS evolution) to reactor operating temperature may thus tend to offset the WPS benefit. If the WPS specimen is loaded while being heated, then the process is called dynamic strain aging, because the straining and aging are taking place concurrently. If aging at elevated temperature follows straining and unloading, the process is simply called strain aging. (However, the term strain aging is often used to refer to either process.)

In his WPS experiments, Andrews tested one strain-aged specimen and one dynamically strain-aged specimen for which the aging temperature was 260 C (500 F), and the aging time was one hour (Andrews 1970), as noted in Table 1. He observed no significant difference in their WPS behavior from specimens which were not strain aged. This strain aging evolution represents saturation of strain aging embrittlement effects in reactor vessel material, since strain aging saturation can be achieved at 204 C (400F) in a matter of minutes (American Society of Metals 1985). Using the statistical WPS model for 100% unloaded data, these strain aged specimens indicated no departure from the WPS benefit of non-strain aged WPS specimens as shown in Figure 5. Therefore, these experiments support applicability of the 100% unload WPS regression in the presence of saturation strain aging.

Recent KAPL/ORNL data (see Table 4) on A508-Class 2 steel examined the effects of strain aging combined with ductile tearing (Macdonald 1995). Five 4T-C(T)s were warm prestressed at 204 C (400 F) at limit load, during which time 0.3 to 0.6 mm (0.013- 0.024 in) of stable crack extension took place. The specimens were then strain aged at 204 C for four hours at about 90% of limit load. While maintaining the strain aging load, the specimens were cooled to -128.9 C (-200 F). Finally, the load was gradually increased at the -128.9 C temperature until fracture occurred slightly above the WPS load. During the final loading, the load vs load line deflection response was linear. This enabled an estimate of K(J) at fracture as K(J) at WPS plus a small linear elastic contribution. The data are shown in Table 4 where "P" is load, "Sy" is yield strength, and "frac" indicates a value at -128.9 C. The fracture loads were at least 7% greater than the WPS load, indicating that the stable tearing and strain aging experienced by these specimens did not cause a significant decrement in WPS benefit. The result of applying the partial unload WPS model to these data is shown in Figure 5. Both plastic zone corrected K (PZC) and K(J) estimates are shown. The observed values of K_{Ifrac} consistently exceeded those of the model. Clearly, the model is conservative for this combination of WPS, strain aging, and ductile tearing. The negative effects of strain aging and ductile tearing were apparently overwhelmed by the intensity of the WPS evolution.

Other investigators have suggested a decrement in WPS benefit due to strain aging (Succop 1970; Haigh 1984; Lidbury 1988). Unfortunately, the information required for the present analysis was not published. Furthermore, the work was carried out on small specimens which underwent considerable plasticity. This may have rendered the results unsuitable for analysis by the present method, as noted for some of the highly plastically deformed Chell et al specimens as discussed earlier. The significant plasticity indicated for some of these WPS strain aging data may also cast doubt on their applicability as discussed next.

Succop, et al reported on tests of A516 Grade 70 and nickel-modified A302-B (Succop 1970). Greater susceptibility to aging was noted for the A516 than the A302-B, and no significant aging effect was noted for aging temperatures below 343 C (650F).

Haigh's report dealt with a silicon-killed carbon-manganese plate (Haigh 1984). All except one specimen experienced ductile tearing during WPS loading, which may affect their applicability. Final fracture toughness of the specimen with no ductile tearing exceeded the baseline fracture toughness by 24%. The other specimens indicated that there was a decrement in WPS benefit due to the onset of ductile tearing during the WPS evolution. However, it would seem difficult to separate the decrement in WPS benefit from that due to strain aging if they are both present in the same experiment.

Lidbury and Birkett's 0.8 inch thick specimen data tended to exhibit ductile tearing during dynamic strain aging (Lidbury 1988). As was just noted, it may be difficult to discriminate how concurrent ductile tearing and strain aging affect the WPS benefit.

In summary, it appears that the effect of strain aging on the WPS benefit is of no consequence for the pressure vessel steels and WPS temperatures used to create the data for Table 1. Ductile tearing, on the other hand, may cause significant damage to the crack tip plastic zone, and thereby decrease WPS benefit.

Full Scale Tests

Full scale WPS tests were conducted by ORNL in the heavy section steel technology (HSST) program. Vessel wall thicknesses were 303mm (6 inches). Thermal shock experiments (TSE's) were cooled rapidly to simulate loss of coolant accident (LOCA) scenarios in which hot coolant is replaced by cold fill water. Pressurized thermal shock experiments (PTSE's) included repressurization after rapid cooling to simulate repressurization after isolation of a large pipe break LOCA. The three experiments discussed below included demonstrations of WPS.

PTSE-1 included a demonstration of WPS (Bryan 1985) for the special case of 0% unloading, called Type I WPS. For this experiment, K_{Iwps}=152 MPa-$m^{1/2}$ (138 ksi-$in^{1/2}$), and at the brittle fracture temperature of interest, K_{Ic}=87.5 MPa-$m^{1/2}$ (79.5 ksi-$in^{1/2}$). At this temperature, the maximum observed K_I without the occurrence of fracture was 153 MPa-$m^{1/2}$ (139 ksi-$in^{1/2}$). The analysis included application of the Chell model from which K_I Chell=153 MPa-$m^{1/2}$ (139 ksi-$in^{1/2}$). The partial unloading regression equation yields a best fit prediction of 162 MPa-$m^{1/2}$ (147 ksi-$in^{1/2}$). Clearly Type I WPS was present and the predictions were both substantiated.

TSE-5A (Cheverton 1985) also included a demonstration of Type I WPS for the case of 0% unloading. For this test, K_{Iwps}=152 MPa-$m^{1/2}$ (138 ksi-$in^{1/2}$), and at the brittle fracture temperature of interest, K_{Ic}=50.0 MPa-$m^{1/2}$ (45.4 ksi-$in^{1/2}$). The maximum observed K_I without the occurrence of fracture was 154 MPa-$m^{1/2}$ (140 ksi-$in^{1/2}$). The partial unloading regression equation yields a best fit prediction of 143 MPa-$m^{1/2}$ (130 ksi-$in^{1/2}$) which is within 1.1 σ of the observed value.

PTSE-2A (Bryan 1987) included a demonstration of WPS with 13% unloading. During WPS and/or reloading, 2.9mm (0.114 in) of stable tearing took place. For this test, K_{Iwps}=195.7 MPa-$m^{1/2}$ (177.9 ksi-$in^{1/2}$), and at the brittle fracture temperature of interest, K_{Ic}=151.6 MPa-$m^{1/2}$ (137.8 ksi-$in^{1/2}$). The material toughness value of K_I at tearing onset=171.0 MPa-$m^{1/2}$ (155.4 ksi-$in^{1/2}$), and the maximum observed K_I at fracture was 198.9 MPa-$m^{1/2}$ (180.8 ksi-$in^{1/2}$). The regression equation yields a best fit prediction of 228.4 MPa-$m^{1/2}$ (207.6 ksi-$in^{1/2}$) which is 3 σ

above the observed value. Apparently there was a decrement in the WPS benefit due to the presence of ductile tearing prior to brittle fracture. In order to account for the effect of tearing, it was assumed that K_{Iwps} could be no greater than K_I at tearing onset because there were no tearing onset data in the database. When this was done, the regression yielded a predicted K_I at fracture of 208.9 (189.9 ksi-in$^{1/2}$) which is 1 σ above the observed value. This demonstrates that the regression model should be restricted to cases in which ductile tearing is excluded. Since these data lie above the lower 2σ estimate of the regression in Figure 6, they appear to support the regression model.

Data Scaled from Reports by Others, and Compilation of All Data Discussed

Hollstein et al (Hollstein 1986), Curry (Curry 1981), and Okamura et al (Okamura 1994) presented graphical data which was scaled and plotted for comparison with the models derived in the present work. These data were not used to adjust the model, due to possible inaccuracies in scaling the data *from* their reports. Figure 7 shows these data, along with all the rest of the data discussed, lie above the lower 2σ estimate of the regressions, except for one KAPL/ORNL datum.

Impact on Brittle Fracture Analysis

If one supposes that the lower 2σ estimate of the regressions is sufficiently conservative, then families of K_{Ifrac} vs normalized temperature for various K_{Iwps} values may be compared with the fracture toughness design curve. For example, consider the lower 2σ estimate for partial unloading, Table 2, compared with the ASME K_{IR} curve in Figure 8. Supposing 150 ksi-in$^{1/2}$ to be the tearing onset limit, the maximum benefit is obtained when K_{Iwps} = 150 ksi-in$^{1/2}$. K_{Ifrac} is clearly a significant improvement over K_{IR}, and is limited to the tearing onset value. If one is unwilling to allow $K_{Ifrac} \geq K_{Iwps}$, then that maximum value may be imposed on K_{Ifrac}, as is shown for K_{Iwps} = 100 ksi-in$^{1/2}$. As one would expect, for sufficiently low values of K_{Iwps} there is virtually no benefit, as is shown for K_{Iwps} = 50 ksi-in$^{1/2}$. K_{Ifrac} is at least equal to K_{IR} since K_{Ifrac} exceeded K_{IC} for all experiments. Finally, one observes that although the experiments all supported Type I WPS (no fracture during cooling until reloading occurred), the regression equations apply to the reload, and are inapplicable to Type I WPS. For example, if $K_I \leq K_{Iwps}$ = 100 ksi-in$^{1/2}$, and no reloading takes place during cooling, then fracture will not occur regardless of the value of K_I compared to K_{Ifrac}.

Conclusions

1. Crack tip 3DEPFE analysis indicated that partially unloaded and completely unloaded data should be treated separately, and that the amount of unloading is unimportant for partially unloaded data.

2. The regression models, which use K_{Iwps} and K_{Ic} as independent variables, better represented the WPS benefit than did the more complicated Chell model.

3. An adequate accounting was made for constraint in the WPS experiments.

4. The subclad flaw data support the use of the partial unload regression model, provided that some care is taken to represent the effect of intact cladding, if present.

5. The effect of strain aging at or below 260 C (500 F) on WPS benefit was of no consequence for the pressure vessel steels and WPS temperatures used to derive the regression models.

6. The presence of ductile tearing precludes the use of the regression models.

7. The regression model for partial unloading accurately predicted the behavior of full scale pressure vessel WPS experiments.

8. Both regression models accurately predicted the behavior of WPS experimental results scaled from articles in which the data were not tabulated.

9. All but one of the 174 experiments considered lie above the lower 2σ estimate of the regressions.

10. Although the experiments all supported Type I WPS (no fracture during cooling until reloading occurred), the regression equations apply to the reload, and are inapplicable to Type I WPS.

Acknowledgments

The authors wish to acknowledge helpful discussions with WR Andrews (The M&P Lab), GG Chell (Southwest Research Institute), JG Merkle (Oak Ridge National Laboratory), and WG Howe, TS Schurman and WW Wilkening (Knolls Atomic Power Laboratory).

References

American Society of Metals, 1985, Metals Handbook Desk Edition, Chapter 4, pg. 81

Andrews, WR, 1970, ASME Journal of Engineering for Industry, pp785-791

Bryan, RH, et al, 1985, PTSE-1, NUREG/ CR-4106, ORNL-6135

Bryan RH, et al, 1987, PTSE-2, NUREG/ CR 4888, ORNL-6377

Chell, GG,1980, Proc. 4th International Conference on Pressure Vessel Technology, Institution of Mechanical Engineers, pp 117-124

Chell, GG, and Haigh, JR, 1986, International Journal of Pressure Vessels and Piping 23, 121-132

Cheverton, RD, et al, 1985, TSE-5, 5A, and 6, NUREG/ CR-4249, ORNL-6163

Curry, DA, 1981, International Journal of Fracture, Vol. 17, No. 3, 335-343

Dieter, GE, Jr, 1961, *Mechanical Metallurgy*, McGraw-Hill, pg 135

Haigh, JR, 1984, Effects of Combined Warm Prestressing, Strain Aging, and Ductile Crack growth on the Toughness and Load-Bearing Capacity of a C-Mn Steel, Central Electricity Generating Board, NWR/SSD/84/0012/N

Hollstein, T, Blauel, JG, Keinzler, R, and Nagel, G, 1986, Nuclear Engineering and Design 94, 233-239

Kaya,AC and Erdogan, F, 1980, International Journal of Fracture 16,171-190

Lidbury, D., and Birkett, P., 1988, Effects of Warm Prestressing on the Transition Toughness Behaviour of an A533 Grade B Class 1 Pressure Vessel Steel, 21st ASTM National Symposium on Fracture Mechanics, Annapolis MD

de Lorenzi, HG, 1982, International Journal of Fracture 19, 183-193

Loss, FJ, Gray, RA, and Hawthorne, JR, 1977, Significance of Warm Prestress to Crack Initiation During Thermal Shock, NRL/NUREG Report 8165

Nichols, RW, 1968, The use of overstressing techniques to reduce the risk of subsequent brittle fracture, British Welding Journal, January, 1968

Okamura, H, Yagawa, G, Hidaka, T, Urabe, Y, Satoh, M, Tomimatsu, M, and Iida, M, 1994, ASME Journal of Pressure Vessel Technology, Vol. 116, 267-273

Pokrovsky, VV, Troshchenko, VT, Kapulenko, VG, Podkol'zin, VY, Fiodorov, VG, and Dragunov, YG, 1994, International Journal of Pressure Vessels and Piping 58, 9-24

Reuter, WG, and Epstein, JS, 1987, ASTM STP 969, 597-619

Shum, DKM, 1993, Preliminary Investigation on the Inclusion of Warm Prestress Effects in Fracture-Margin Assesment of Reactor Vessels, NUREG CR-5946, ORNL/TM-12236, RF

Stonesifer, RB, Rybicki, EF, and McCabe, DE, 1989Warm Prestress Modeling: Comparison of Models and Experimental Results, NUREG/ CR-5208, MEA-2305

Succop, LN, Pense, AW, and Stout, RD, 1970, The Effects of Warm Overstressing on Pressure Vessel Steel Properties, Welding Journal Research Supplement, August, 1970

Prin. Author	Spec. I.D.	KI frac ksi-in$^{1/2}$	K I Chell ksi-in$^{1/2}$	KIwps* ksi-in$^{1/2}$	Fracture* Toughness ksi-in$^{1/2}$	unload %	a, in	Sy, ksi	KI frac*, PZC ksi-in$^{1/2}$	KImin* ksi-in$^{1/2}$
Andrews	LCF	70.20	88.68	65.00	43.70	0.00	0.64	140.00	70.98	65.00
Andrews	LCF	111.30	133.25	104.60	43.70	0.00	0.64	140.00	114.48	104.60
Andrews	LCF	68.10	71.68	59.40	57.00	0.00	0.64	74.00	70.75	59.40
Andrews	LCF	110.50	123.75	105.60	57.00	0.00	0.64	74.00	123.05	105.60
Andrews	LCF	82.10	96.26	76.60	56.50	0.00	0.64	64.00	88.68	76.60
Andrews	LCF	107.00	137.61	112.10	51.60	20.00	0.64	61.00	124.99	89.68
Andrews	LCF	67.50	79.33	61.40	51.60	0.00	0.64	61.00	71.40	61.40
Andrews	LCUF	55.00	81.82	65.00	43.70	100.00	0.64	140.00	55.37	0.00
Andrews	LCUF	81.60	104.42	105.60	43.70	100.00	0.64	140.00	82.83	0.00
Andrews	LCUF	75.00	104.60	105.80	43.70	100.00	0.64	140.00	75.95	0.00
Andrews	LCUF	99.90	103.89	103.70	57.00	100.00	0.64	74.00	108.88	0.00
Andrews	LCUF	77.50	97.39	104.60	37.10	100.00	0.64	129.00	78.74	0.00
Andrews	LCUF	97.40	108.41	102.80	56.50	100.00	0.64	64.00	108.97	0.00
Andrews	LCUF	71.70	89.01	72.70	56.50	100.00	0.64	64.00	75.96	0.00
Andrews	LCUF	65.00	86.36	70.40	51.60	100.00	0.64	61.00	68.46	0.00
Andrews	LCUF, aged	65.30	87.13	69.00	51.60	100.00	0.64	61.00	68.81	0.00
Andrews	LUCF	49.40	80.13	62.30	43.70	100.00	0.64	140.00	49.67	0.00
Andrews	LUCF	72.80	105.55	108.20	43.70	100.00	0.64	140.00	73.67	0.00
Andrews	LUCF	60.20	104.25	104.30	43.70	100.00	0.64	140.00	60.69	0.00
Andrews	LUCF	72.10	92.56	77.00	56.50	100.00	0.64	64.00	76.43	0.00
Andrews	LUCF	65.40	97.79	90.60	51.60	100.00	0.64	61.00	68.93	0.00
Andrews	LUCF, aged	50.70	83.49	65.90	51.60	100.00	0.64	61.00	52.29	0.00
Chell	b1	15.36	13.76	11.45	14.09	100.00	1.00	132.70	15.37	0.00
Chell	a2	17.00	16.08	17.55	13.27	100.00	1.00	213.50	17.00	0.00
Chell	b5	23.64	21.07	31.36	14.09	100.00	1.00	132.70	23.66	0.00
Chell	b6	19.09	19.05	24.27	14.09	100.00	1.00	132.70	19.10	0.00
Chell	b7	18.82	18.97	24.00	14.09	100.00	1.00	132.70	18.83	0.00
Chell	b12	31.09	31.41	31.36	14.09	50.00	1.00	132.70	31.14	15.68
Chell	b15	24.00	26.27	21.36	14.09	0.00	1.00	132.70	24.02	21.36
Chell	b16	16.09	17.14	12.00	14.09	0.00	1.00	132.70	16.10	12.00
Chell	b18	35.09	36.59	31.73	14.09	0.00	1.00	132.70	35.16	31.73
Loss	bu7	64.36	58.52	53.91	62.57	30.00	1.26	78.00	65.35	37.74
Loss	bu3	65.27	61.01	56.45	62.57	32.00	1.26	78.00	66.30	38.39
Loss	bu4	63.55	59.50	54.91	62.57	33.00	1.26	78.00	64.50	36.79
Loss	bu6	68.91	63.10	61.45	62.57	100.00	1.26	78.00	70.13	0.00
Loss	ca8	71.36	62.33	59.91	62.57	100.00	1.26	78.00	72.72	0.00
Loss	bu11	86.09	87.52	83.18	62.57	51.00	1.26	78.00	88.50	40.76
Loss	bu12	90.27	84.36	80.18	62.57	53.00	1.26	78.00	93.06	37.69
Loss	bu8	64.27	64.42	58.91	55.67	37.00	1.26	82.00	65.16	37.11
Loss	jv6	65.45	65.95	59.82	55.67	28.00	1.26	82.00	66.39	43.07
Loss	jv7	61.55	58.56	58.00	55.67	100.00	1.26	82.00	62.32	0.00
Loss	ca1	67.82	57.25	55.64	55.67	100.00	1.26	82.00	68.86	0.00
Loss	ca4	80.45	83.24	77.00	55.67	52.00	1.26	82.00	82.22	36.96
Loss	ca9	78.55	81.08	74.91	55.67	40.00	1.26	82.00	80.18	44.95
Loss	ca10	58.73	62.70	53.82	37.07	28.00	1.26	86.00	59.34	38.75
Loss	ca12	47.64	47.35	56.64	37.07	100.00	1.26	86.00	47.96	0.00
Loss	ca3	81.45	81.10	78.00	37.07	56.00	1.26	86.00	83.11	34.32
Loss	ca11	53.55	61.97	53.55	25.67	56.00	1.26	86.00	54.01	23.56
Loss	jv3	59.27	67.06	64.00	25.67	66.00	1.26	86.00	59.90	21.76
Loss	ca2	66.27	73.04	76.64	25.67	71.00	1.26	86.00	67.16	22.22
Loss	ju3	105.00	105.47	101.18	62.57	51.00	2.52	78.00	107.16	49.58
Loss	ju1	73.55	70.29	76.91	62.57	100.00	2.52	78.00	74.28	0.00
Loss	jx4	76.36	76.57	72.18	62.57	49.00	2.52	78.00	77.18	36.81
Loss	jx2	94.27	82.89	108.82	62.57	100.00	2.52	78.00	95.83	0.00
Loss	jv2	108.09	108.06	108.09	62.57	63.00	2.52	78.00	110.45	39.99
Loss	jx1	79.64	81.85	75.82	54.17	51.00	2.52	82.00	80.48	37.15
Loss	jw4	73.55	74.85	108.55	54.17	100.00	2.52	82.00	74.21	0.00
Loss	jx3	68.91	64.06	77.00	54.17	100.00	2.52	82.00	69.45	0.00

* plastic zone corrected value; mm=in*25.4; KN=kips*4.44: MPa=ksi*6.894; KPa-m=lb/in*0.175; MPa-m$^{1/2}$=ksi-in$^{1/2}$*1.1

Table 1. Warm Prestressing Data, page 1 of 2

Prin. Author	Spec. I.D.	KI frac ksi-in$^{1/2}$	K I Chell ksi-in$^{1/2}$	KIwps* ksi-in$^{1/2}$	Fracture* Toughness ksi-in$^{1/2}$	unload %	a, in	Sy, ksi	KI frac, PZC ksi-in$^{1/2}$	KImin* ksi-in$^{1/2}$
Loss	jv1	107.18	102.01	108.00	54.17	66.00	2.52	82.00	109.26	36.72
Loss	ju2	102.27	102.44	108.09	54.17	66.00	2.52	82.00	104.07	36.75
Loss	jw2	98.00	96.41	109.73	39.17	67.00	2.52	86.00	99.43	36.21
Loss	jw3	57.27	61.39	108.27	39.17	100.00	2.52	86.00	57.55	0.00
Loss	ju4	79.73	84.21	87.55	39.17	64.00	2.52	86.00	80.49	31.52
KAPL/ORNL	u01	85.17	95.14	80.65	60.20	75.00	0.84	109.00	86.95	20.16
KAPL/ORNL	u29	102.96	114.28	99.99	60.20	34.00	0.84	109.00	106.13	65.99
KAPL/ORNL	u22	117.26	133.82	119.63	60.20	59.00	0.84	109.00	122.02	49.05
KAPL/ORNL	u08	96.62	88.86	81.33	69.50	23.00	0.84	84.00	101.15	62.62
KAPL/ORNL	u14	116.04	107.84	100.58	69.50	56.00	0.84	84.00	124.14	44.26
KAPL/ORNL	u20	120.74	127.52	120.38	69.50	79.00	0.84	84.00	129.94	25.28
KAPL/ORNL	u06	133.40	98.84	81.38	98.80	48.00	0.84	76.00	149.50	42.32
KAPL/ORNL	u12	124.70	105.74	100.90	98.80	77.00	0.84	76.00	137.54	23.21
KAPL/ORNL	u27	122.27	123.07	118.59	98.80	40.00	0.84	76.00	134.30	71.15
KAPL/ORNL	u07	90.71	96.27	81.79	60.20	23.00	0.84	109.00	92.86	62.98
KAPL/ORNL	u13	112.03	114.59	100.30	60.20	55.00	0.84	109.00	116.16	45.14
KAPL/ORNL	u19	114.41	134.24	121.00	60.20	80.00	0.84	109.00	118.82	24.20
KAPL/ORNL	u05	92.45	88.84	81.31	69.50	48.00	0.84	84.00	96.40	42.28
KAPL/ORNL	u11	110.18	108.36	101.10	69.50	78.00	0.84	84.00	117.05	22.24
KAPL/ORNL	u26	125.33	128.02	120.89	69.50	41.00	0.84	84.00	135.72	71.33
KAPL/ORNL	u03	118.21	98.84	86.24	98.80	75.00	0.84	76.00	128.97	21.56
KAPL/ORNL	u18	108.76	105.65	100.80	98.80	35.00	0.84	76.00	116.97	65.52
KAPL/ORNL	u24	116.89	124.53	120.07	98.80	59.00	0.84	76.00	127.26	49.23
KAPL/ORNL	u04	91.13	95.53	81.04	60.20	47.00	0.84	109.00	93.32	42.95
KAPL/ORNL	u10	85.07	115.58	101.30	60.20	77.00	0.84	109.00	86.83	23.30
KAPL/ORNL	u25	122.37	134.96	120.77	60.20	40.00	0.84	109.00	127.82	72.46
KAPL/ORNL	u02	105.54	88.72	81.18	69.50	74.00	0.84	84.00	111.52	21.11
KAPL/ORNL	u17	109.39	109.16	101.91	69.50	65.00	0.84	84.00	116.10	35.67
KAPL/ORNL	u23	114.88	127.77	120.64	69.50	60.00	0.84	84.00	122.72	48.26
KAPL/ORNL	u09	91.50	98.84	81.44	98.80	23.00	0.84	76.00	96.23	62.71
KAPL/ORNL	u15	118.58	105.94	101.10	98.80	56.00	0.84	76.00	129.45	44.48
KAPL/ORNL	u28	114.56	124.42	119.96	98.80	81.00	0.84	76.00	124.28	22.79
Stonesifer	1	146.80	178.48	173.00	113.00	100.00	3.93	68.45	151.82	0.00
Stonesifer	2	161.00	179.61	175.18	113.00	100.00	3.93	68.45	167.69	0.00
Stonesifer	3	164.20	180.83	177.64	113.00	100.00	3.93	68.45	171.32	0.00
Stonesifer	4	144.70	178.94	173.91	113.00	100.00	3.93	68.45	149.50	0.00
Stonesifer	5	157.30	179.61	175.27	113.00	100.00	3.93	68.45	163.52	0.00
Stonesifer	6	157.00	182.76	181.45	113.00	100.00	3.93	68.45	163.19	0.00
Stonesifer	7	144.30	182.91	178.27	113.00	100.00	3.93	68.45	149.06	0.00
Stonesifer	8	147.60	180.83	177.64	113.00	100.00	3.93	68.45	152.70	0.00
Stonesifer	9	149.00	181.49	178.91	113.00	100.00	3.93	68.45	154.26	0.00
Stonesifer	10	161.00	180.78	177.55	113.00	100.00	3.93	68.45	167.69	0.00
Stonesifer	11	124.40	138.00	174.36	62.09	100.00	3.93	77.88	126.71	0.00
Stonesifer	12	136.00	138.16	174.73	62.09	100.00	3.93	77.88	139.03	0.00
Stonesifer	13	134.60	138.28	175.00	62.09	100.00	3.93	77.88	137.54	0.00
Stonesifer	14	109.60	138.12	174.80	62.09	100.00	3.93	77.88	111.17	0.00
Stonesifer	15	135.30	137.97	174.18	62.09	100.00	3.93	77.88	138.28	0.00
Stonesifer	16	124.10	138.75	176.18	62.09	100.00	3.93	77.88	126.39	0.00
Stonesifer	17	113.90	138.48	175.55	62.09	100.00	3.93	77.88	115.66	0.00
Stonesifer	18	130.20	139.11	177.09	62.09	100.00	3.93	77.88	132.85	0.00
Stonesifer	19	133.50	138.48	175.55	62.09	100.00	3.93	77.88	136.36	0.00
Stonesifer	20	119.00	138.60	175.82	62.09	100.00	3.93	77.88	121.01	0.00
Stonesifer	21	151.20	178.45	168.10	62.09	33.00	3.93	77.88	155.40	112.63
Stonesifer	22	153.40	184.74	174.40	62.09	33.00	3.93	77.88	157.79	116.85
Stonesifer	23	163.50	185.64	175.30	62.09	33.00	3.93	77.88	168.84	117.45
Stonesifer	24	155.20	182.05	171.70	62.09	33.00	3.93	77.88	159.75	115.04
Stonesifer	25	162.80	182.25	171.90	62.09	33.00	3.93	77.88	168.07	115.17
Stonesifer	26	155.20	179.05	168.70	62.09	33.00	3.93	77.88	159.75	113.03
Stonesifer	27	162.00	180.25	169.90	62.09	33.00	3.93	77.88	167.19	113.83
Stonesifer	28	166.60	187.84	177.50	62.09	33.00	3.93	77.88	172.27	118.93
Stonesifer	29	165.00	182.75	172.40	62.09	33.00	3.93	77.88	170.50	115.51

* plastic zone corrected value; mm=in*25.4; KN=kips*4.44: MPa=ksi*6.894; KPa-m=lb/in*0.175; MPa-m$^{1/2}$=ksi-in$^{1/2}$*1.1

Table 1. Warm Prestressing Data, page 2 of 2

% Unload	constant	K_{Iwps}	K_{Ic}	Kmin	K_{Iwps} x K_{Ic}	K_{Iwps} x Kmin	K_{Ic} x Kmin	R^2	SE (σ)
0 - 100	Chell's Model							0.89	13.5
0 -100	-8.41	0.55	0.85	0.34	-1.196e-03	1.527e-03	-4.071e-03	0.94	9.61
100	Chell's Model							0.92	12.7
100	-2.76	0.51	0.65	-	-	-	-	0.96	9.24
0 - 80	Chell's Model							0.89	12.5
0 - 80	-2.02	0.79	0.50	-	-	-	-	0.94	8.79

Table 2. Correlation Parameter Coefficients and Comparison of WPS Models

ID	temp, F	path	carbon insert	WPS K(J) ksi-in$^{1/2}$	minload / WPS load	K_{Ic} from unclad, ksi-in$^{1/2}$	model -2σ ksi-in$^{1/2}$	Fracture K(J) ksi-in$^{1/2}$	Fracture Load, kips
C1	-200.00	LUCF	yes	69.9	1/3	60.20	65.8	67.4	193.3
C2	0.00	LUCF	no	69.4	1/3	98.80	84.7	115.3	242.8
C3	-200.00	LUCF	no	69.9	2/3	60.20	65.8	81.5	220.6
C4	0.00	LUCF	yes	70.4	2/3	98.80	85.5	185.8	281.4
C5	-200.00	LCUF	yes	70.4	1/3	60.20	66.2	85.7	228.4
C6	0.00	LCUF	no	71.0	1/3	98.80	86.0	92.9	222.4
C7	-200.00	LCUF	yes	70.4	1/3	60.20	66.2	83.6	224.6
C8	0.00	LCUF	no	71.0	2/3	98.80	86.0	90.5	219.8

Notes

1. WPS load = 180 kips
2. mm = in x 25.4; KN = kips x 4.44; MPa = ksi x 6.894; KPa-m = lb/in x 0.175; MPa-m$^{1/2}$ = ksi-in$^{1/2}$ x 1.1
3. K_{Ic} is K_I at fracture of control specimens as noted in text.

Table 3. Analysis of Subclad Flaw, Warm Prestressed Beams

specimen code	a_o, in	B, in	W, in	P_{max} wps, kips	Δa wps, in	a_{wps}, in	a_{wps}/ W
1	4.9580	4.00	8.00	119.20	0.0132	4.9712	0.6214
2	4.9060	4.00	8.00	115.60	0.0135	4.9195	0.6149
3	5.2190	4.00	8.00	100.50	0.0137	5.2327	0.6541
4	4.9280	4.00	8.00	120.00	0.0236	4.9516	0.6190
5	4.8580	4.00	8.00	135.10	0.0201	4.8781	0.6098

specimen code	K elas wps, ksi-$in^{1/2}$	Sy, wps ksi	K_I wps, pzc ksi-$in^{1/2}$	J wps lb/in	K(Jwps) ksi-$in^{1/2}$	P frac, -200F, kips	P frac / P wps
1	156.85	72.00	161.18	1673.00	224.00	127.00	1.07
2	148.11	72.00	151.78	1452.00	209.00	125.00	1.08
3	152.56	72.00	156.33	1823.00	234.00	110.00	1.09
4	156.31	72.00	160.61	2067.00	249.00	128.00	1.07
5	169.50	72.00	175.11	2128.00	253.00	145.00	1.07

specimen code	K frac, ksi-$in^{1/2}$	Sy, frac ksi	K_I frac, PZC, ksi-$in^{1/2}$	K_{Ic}, -200F ksi-$in^{1/2}$	Model, PZC ksi-$in^{1/2}$	K(J) frac ksi-$in^{1/}$	Model, K(J) ksi-$in^{1/}$
1	167.11	103.00	169.63	29.50	140.06	234	190
2	160.15	103.00	162.39	29.50	132.64	221	178
3	166.98	103.00	169.36	29.50	136.23	248	198
4	166.73	103.00	169.23	29.50	139.61	259	209
5	181.92	103.00	185.24	29.50	151.07	265	213

Note: mm = in x 25.4; KN = kips x 4.44; MPa = ksi x 6.894; KPa-m = lb/in x 0.175; MPa-$m^{1/2}$ = ksi-$in^{1/2}$ x 1.1

Table 4. KAPL/ORNL WPS Data with Strain Aging and Ductile Tearing

Figure 1a. Complete and Partial Unloading, Chell Model

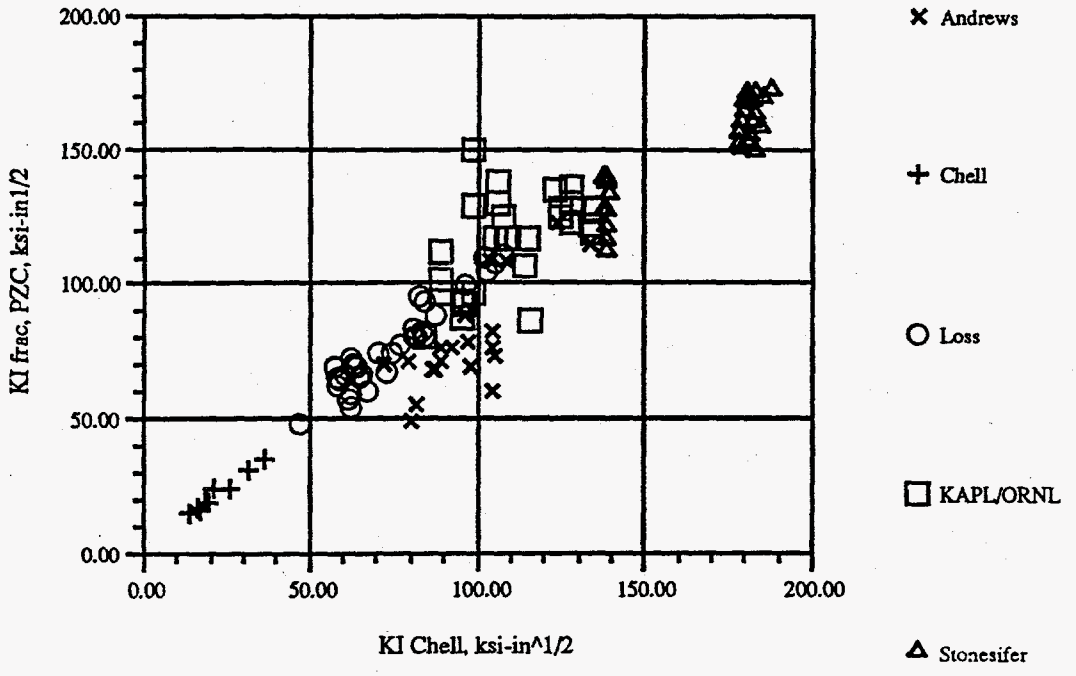

Figure 1b. Complete and Partial Unloading, Regression Model

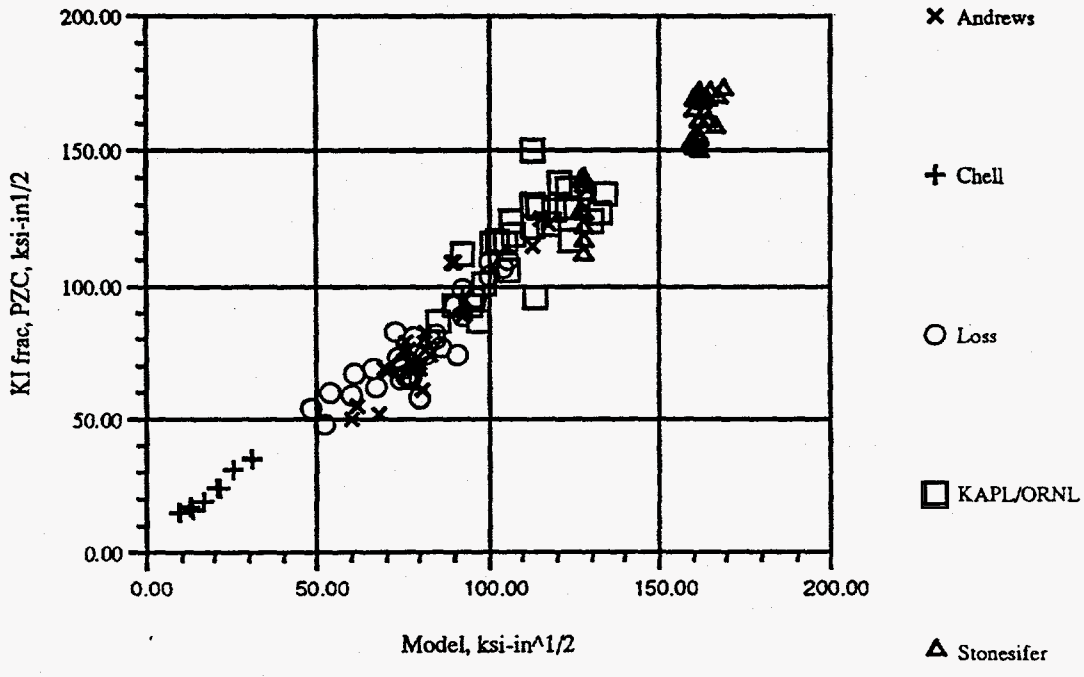

Figure 2. Complete and Partial Unloading Modeled Separately

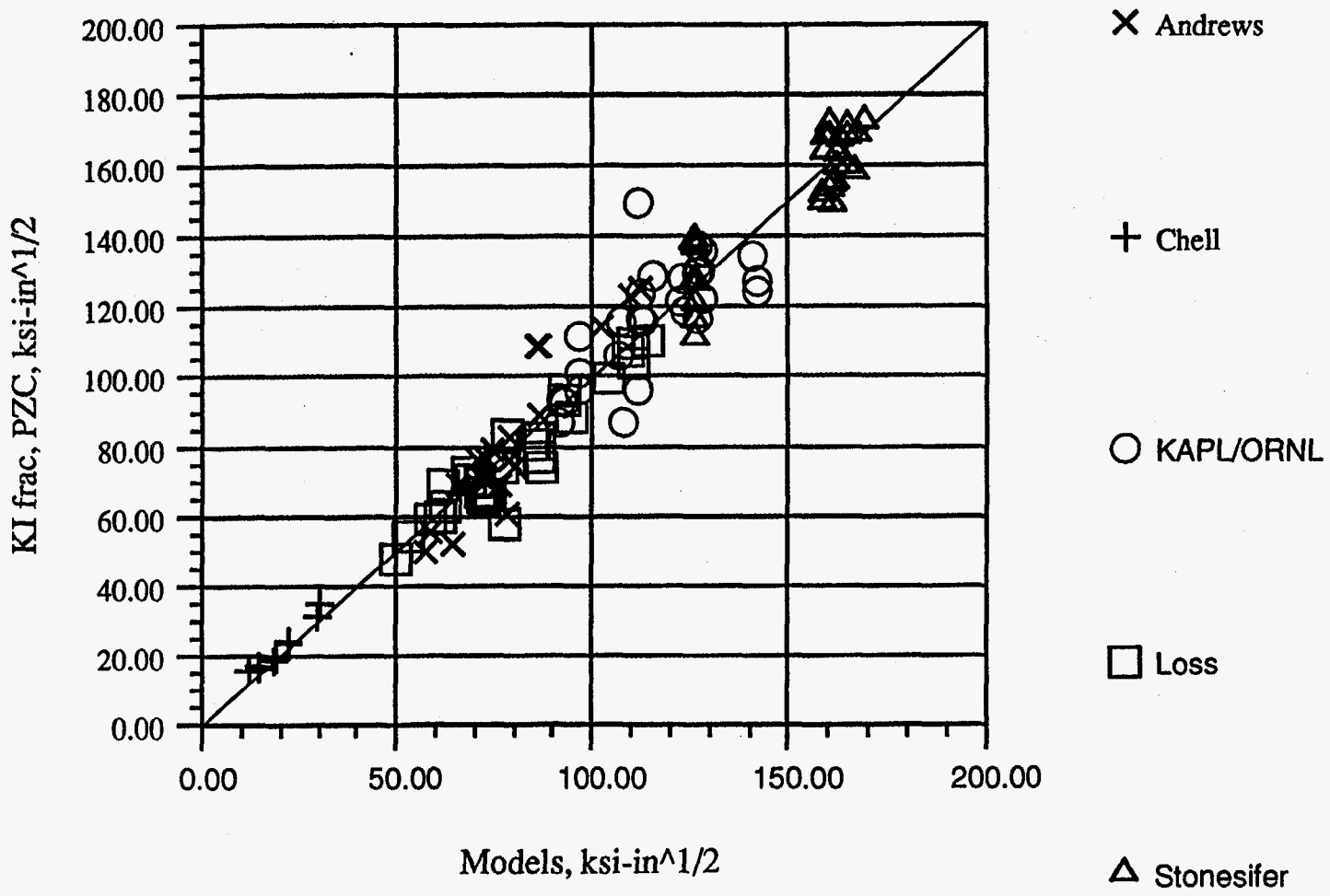

14/25

Figure 3. Crack Opening Stress During Unloading

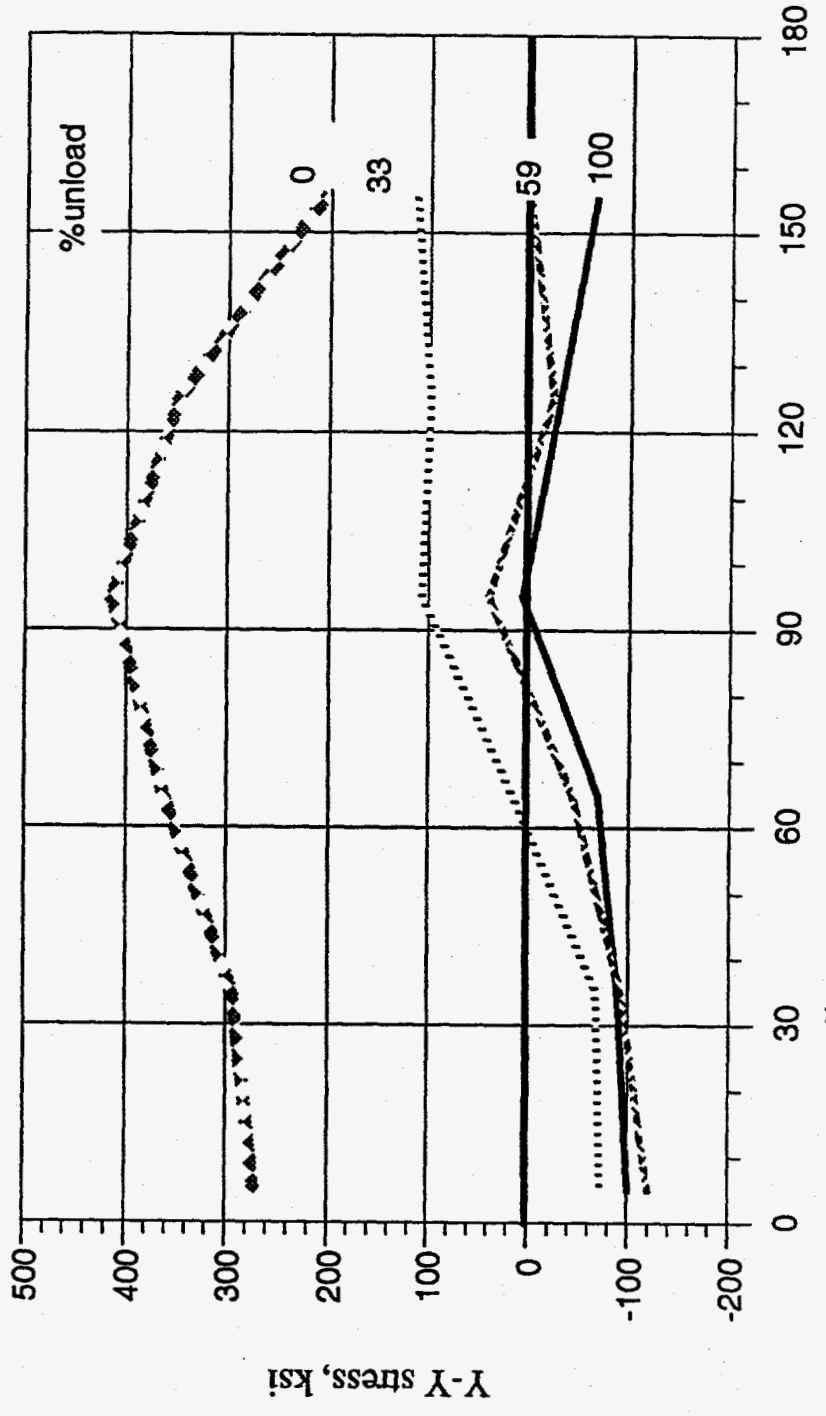

Figure 4. Partial Unload Data and Subclad Flaw Data

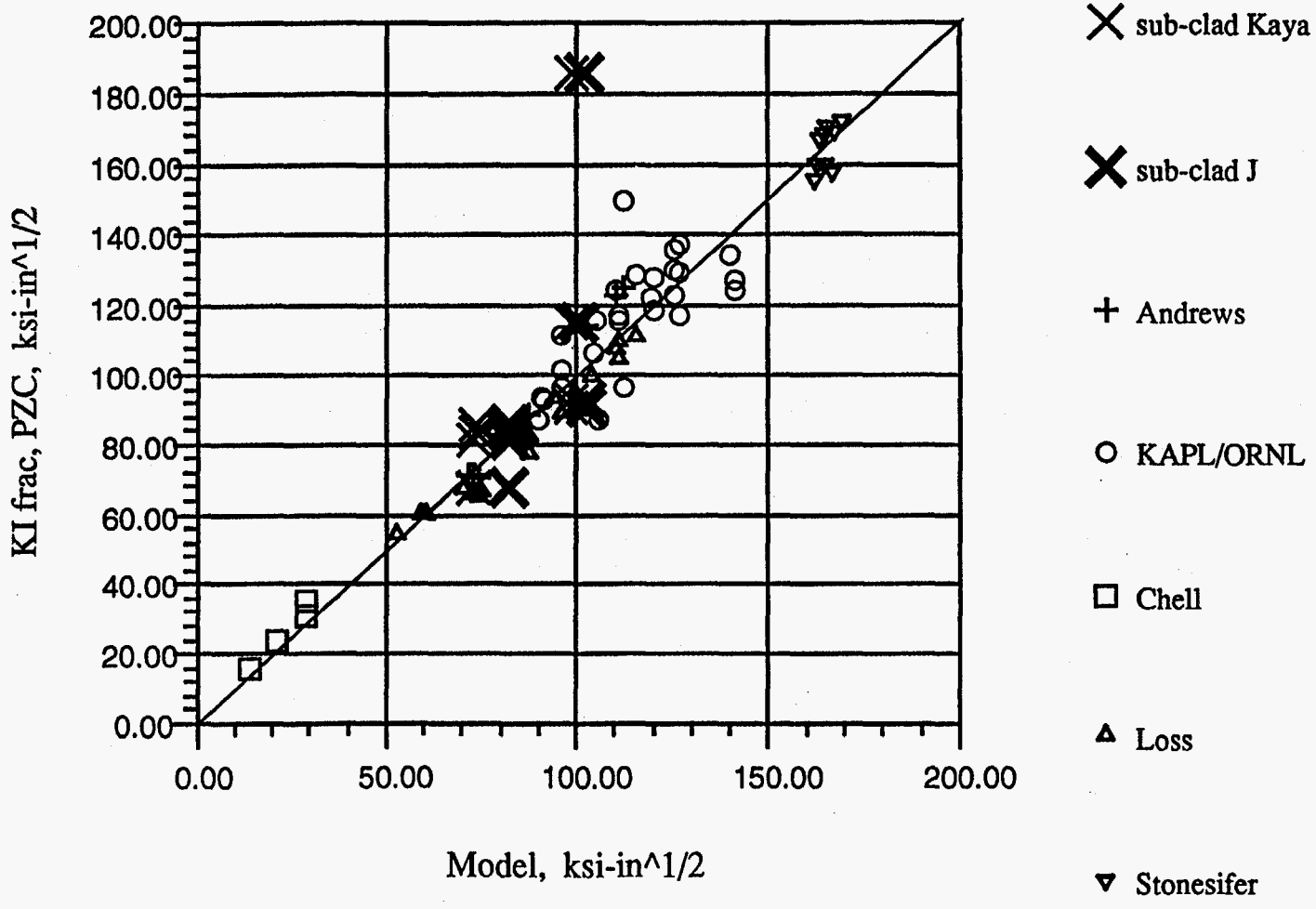

18/25

Figure 5. Strain Aged Data and Partial and Complete Unloading Data

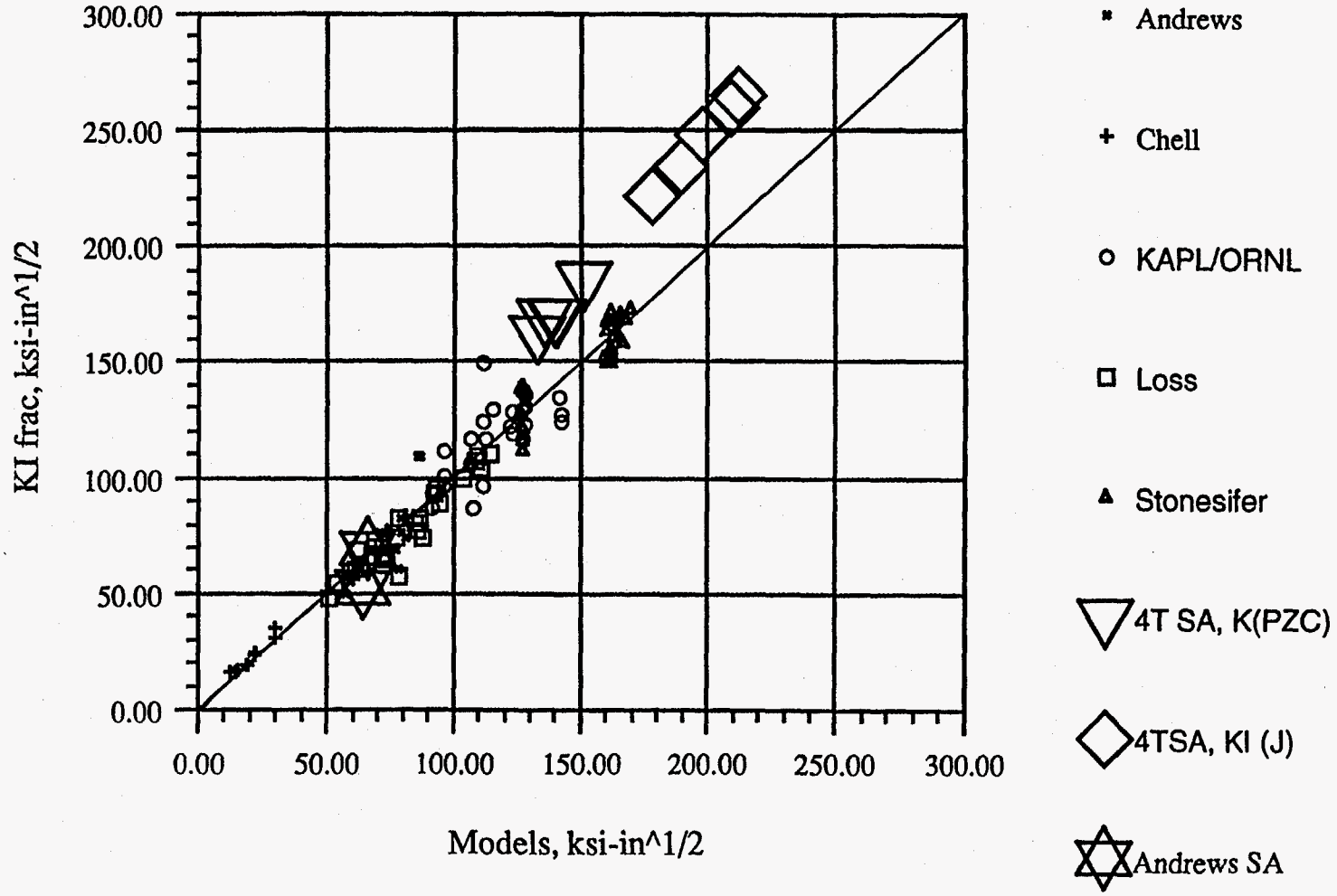

Figure 6 . Partial Unloading Data and HSST Data

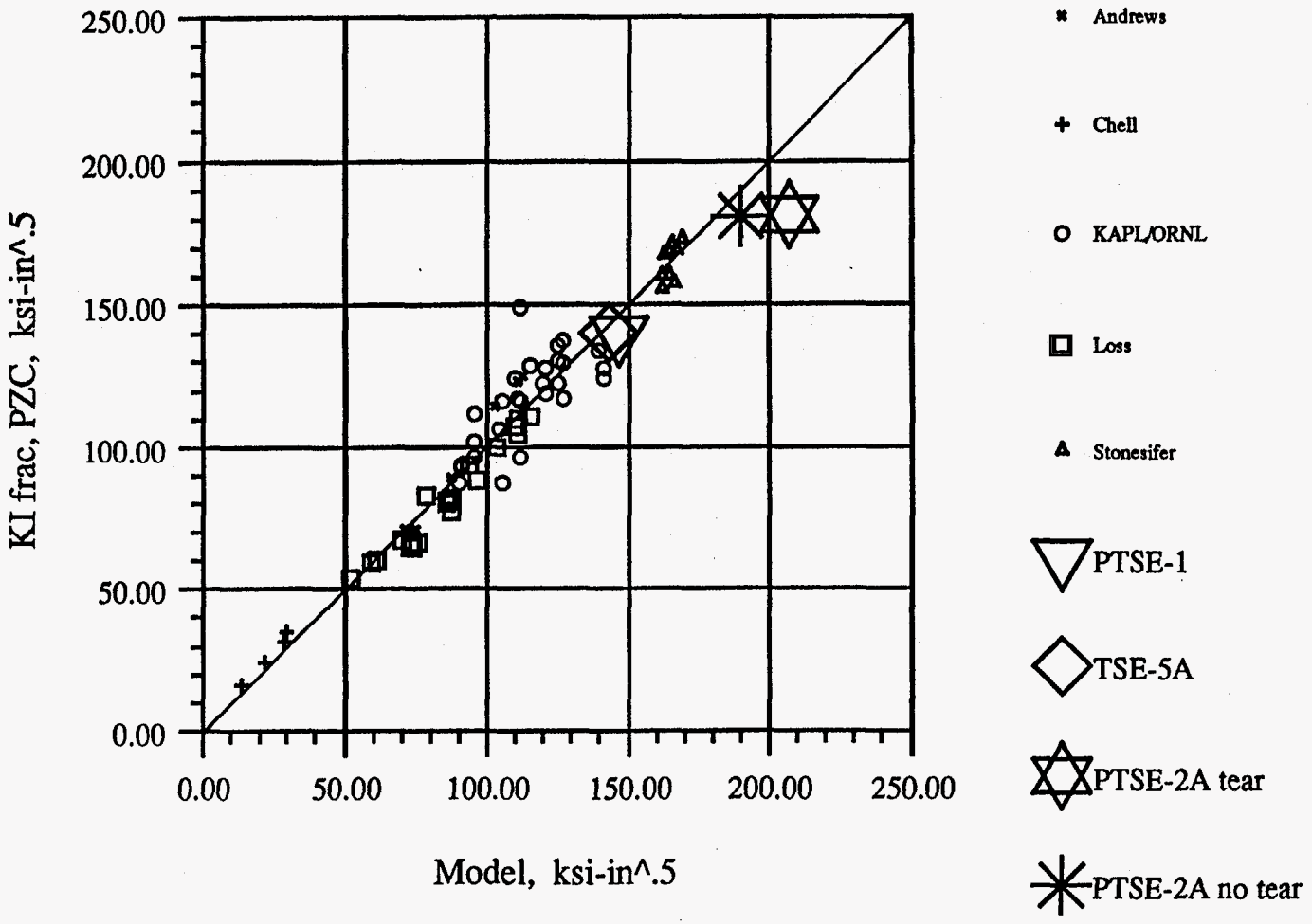

Figure 7. All 174 Data Points, Complete and Partial Unloading

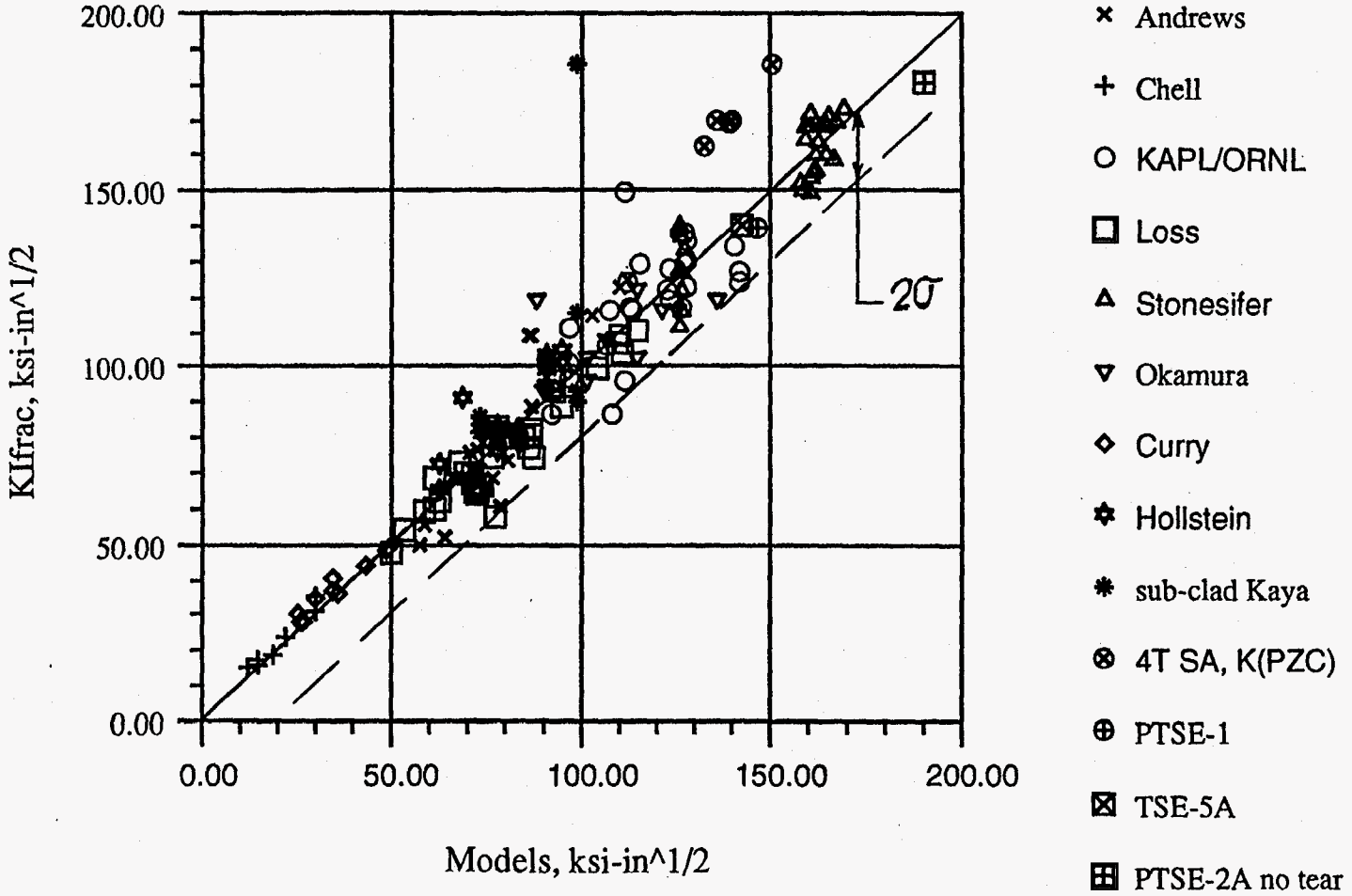

Figure 8 . WPS Benefit to ASME KIr Curve, Partial Unloading 2 Sigma

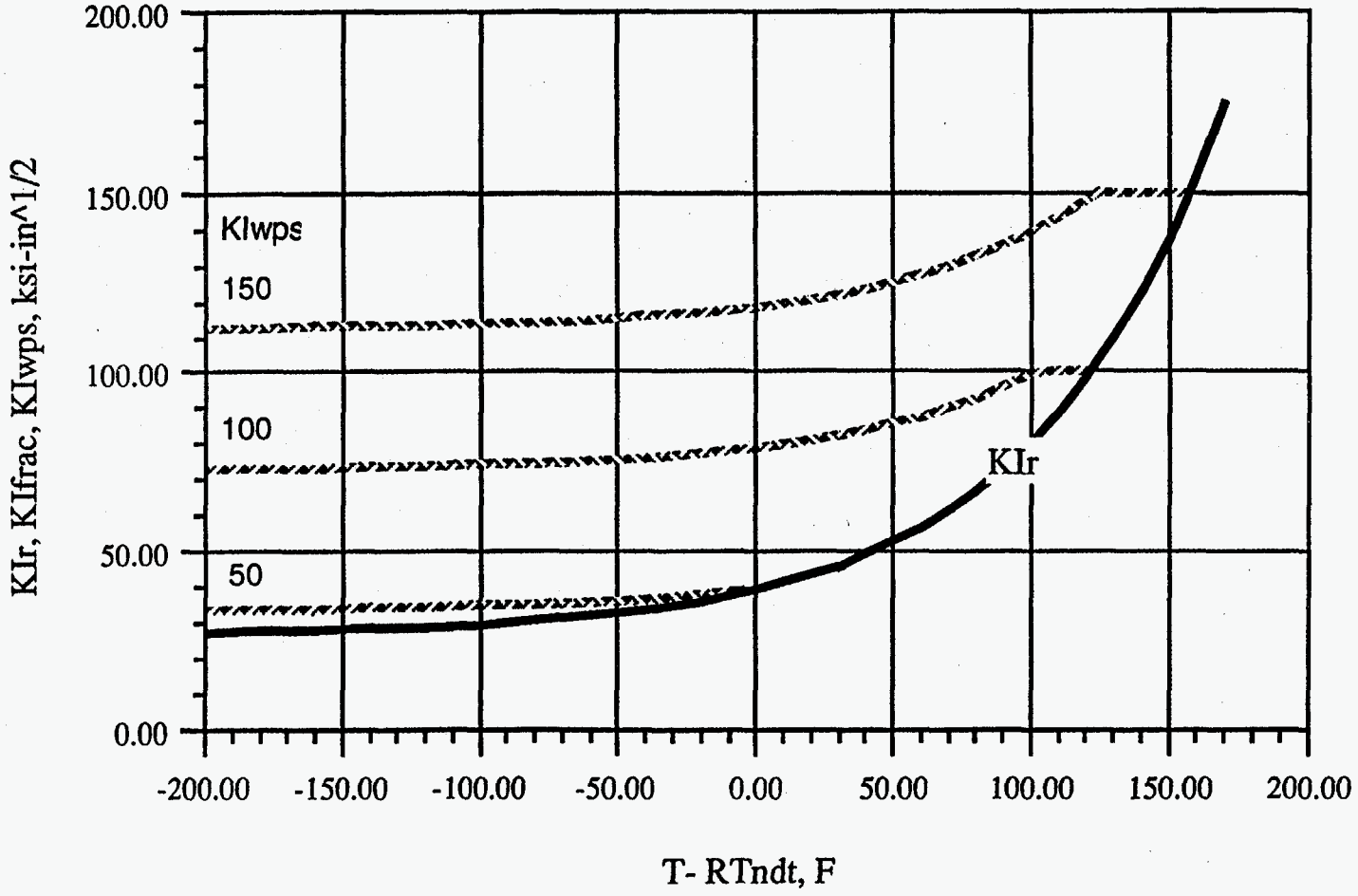

2/2/25

APPENDIX A: KAPL/ORNL TEST PROGRAM SUMMARY

A.1 INTRODUCTION

The KAPL/ORNL unclad warm-prestress (WPS) experimental program consisted of a total of 38 tests in two groups. The first group was a control matrix of 6 specimens tested under isothermal conditions at three different temperatures, - 129 C, -73 C, and - 18 C. These tests were conducted to provide a baseline for evaluation of the fracture toughness obtained from the subsequent WPS tests. The second group, the WPS tests, consisted of 32 tests with failure temperature, WPS load magnitude, and test histogram being the independent variables. Three types of WPS histograms were used. These are shown schematically in Fig. Al and were defined as Load-Unload-Cool-Fracture (LUCF), Load-Cool-Unload-Fracture (LCUF), and LINEAR. The WPS temperature was a constant 149 C for all tests. Data for the unclad WPS tests were shown in Table 1. Eight clad WPS beams with sub-clad flaws were similarly tested, and the data were shown in Table 3.

A.2 SPECIMEN FABRICATION

The unclad test specimens were beams 914-mm long, 102-mm deep, and 127-mm wide. They were of a composite design in which only the test section was fabricated from pedigreed material. The dimensions and general layout of the test sections are shown in Fig. A2. Reusable beam arms were electron-beam (EB) welded to the ends of the test section to form the full beam configuration. Blanks for the test sections were taken from the residual parts of a test cylinder, ASTM A508 Class 2 materials that had been used in prior thermal-shock tests.

The unclad blanks were all machined into test sections with dimensions as shown in Fig. A2. The flaw was ram electron discharge machined into the top surface of the test section in the shape of a semi-ellipse 76.2-mm. long and 19.1-mm deep. After machining, the test sections were post-weld-heat-treated (PWHT) at 621 C for 30 hours using argon purge to minimize oxide buildup. After EB welding the beam arms onto the test section, final machining was performed to remove the EB weld fixtures and weld buildup.

The clad specimens were of the same geometry as the unclad with the exception of an additional 0.2 inch layer of cladding which was deposited after fatigue pre-cracking. In some cases, as indicated in Table 2, a carbon wafer was inserted in the flaw prior to cladding. The cladding was a 3-wire 308-309 stainless steel weld deposit.

A.3 INSTRUMENTATION

Each beam was fully instrumented to measure crack mouth-opening-displacement (CMOD), surface strain, load-line displacement (LLD), and temperature. Three clip gages were located along the flaw mouth, one on the specimen longitudinal centerline, and one 10.1 mm each side of the centerline. Four foil type strain gages oriented in the specimen longitudinal direction were used to measure surface deformation. A 2447-kN load cell was used to measure load during each test. Also, stroke, or test machine actuator movement, was measured through the test machine controller. These stroke measurements were an accurate indication of LLD for the beam. On the group of isothermal tests, a direct current linearly variable differential transducer was mounted to measure LLD directly. However, for the WPS tests, the entire beam was fully enclosed in an environmental chamber, so direct LLD measurements could not be made.

Temperatures were measured using contact thermocouples (TC). Up to eight TCs were mounted on the surface of the test section. An additional TC was inserted into the center of the test section through a side hole that had originally been designed to mount one of the load-line displacement instruments. This TC made contact with the material near the center of the block and was used for control of the experiment. The data were continuously recorded and stored on magnetic media for all tests. The clad beams included additional instrumentation to track cladding deformation.

A.4 TEST PROCEDURES

The procedures contained in ASTM E399 were used as guidelines for these tests, although they do not apply explicitly to the semi-elliptic flaw configuration. After the specimen was instrumented, it was mounted in a four-point bend test fixture, as shown schematically in Fig. A3. The specimen was fatigue precracked at room temperature using CMOD change-in-compliance measurements to determine the amount of crack growth. Development tests were performed to establish the final test procedures to yield the specified amount of crack growth (about 1.3 mm). Two development specimens were tested at room temperature where a history of CMOD compliance versus number of cycles was obtained. The specimens were then broken apart and the amount of crack growth measured. From these data the number of cycles to obtain a specified amount of crack growth was determined. The general fatigue pre-cracking for the control matrix and WPS specimens was performed in two phases. In Phase 1, the crack was grown to approximately 98% of its final length. The specimen was cycled over the range 89 kN to 400 kN, yielding a maximum elastically calculated stress intensity factor and stress intensity factor range of 50 MPa$\sqrt{m}$ and 40 MPa$\sqrt{m}$, respectively. In Phase 2, the maximum load was reduced to 245 kN, yielding a maximum stress intensity factor and stress intensity factor range of 31 MPa$\sqrt{m}$ and 20 MPa$\sqrt{m}$, respectively. Fatigue crack growth was continued until the desired amount of compliance change was measured, indicating the specified crack growth had been achieved. The procedure was continued by making post-test measurements of fatigue crack growth on all specimens in the control matrix tests. As noted earlier, a 0.2 inch layer of cladding was deposited after fatigue pre-cracking the clad beams.

After fatigue pre-cracking, in situ instrumentation checks were performed, and the specimen was prepared for the fracture portion of the test. For the control matrix tests, a special liquid nitrogen (LN_2) manifold was installed, the specimen was thermally insulated, the fixture was re-aligned to assure proper load point contact, and a pre-load of approximately 22-kN was applied and held under machine load-control to maintain this alignment. The specimen was then cooled to the test temperature and held for a minimum of 20 minutes to establish isothermal conditions in the test section. The specimen was then loaded to failure under displacement-control at a rate of 0.003-Hz based on a cyclic amplitude of 20 mm.

The WPS tests varied from this procedure because of additional equipment requirements. After fatigue pre-cracking, electric heaters were mounted on the specimen, the LN_2 manifold was installed, and an environmental chamber that completely enclosed the specimen was put in place. The specimen was than final aligned and pre-loaded to 22-kN. Holding load constant, the specimen was heated to the WPS temperature of 149 C. For a load-unload-cool-fracture (LUCF) test, a stable WPS temperature was established and the specified load-unload cycle was applied at a rate of 0.003-Hz using a test machine generated displacement haversine function. Using load-control to maintain constant load, the specimen was cooled to the fracture temperature, and the fracture phase was conducted as described above. For a load-cool-unload-fracture (LCUF) test, the specimen was loaded using a load-control ramp function. The load was held constant during cool-down to the fracture temperature. The load was lowered to the pre-load value, and the fracture phase was conducted as noted above. For the LINEAR test, the WPS and failure sequences of the test were the same as for the LCUF histogram. However, the LINEAR test utilized a special controller that maintained a linear relationship between the specimen temperature change and the applied load change. During the fracture portion of all tests, all instrumentation was scanned at 0.1 second intervals to assure good definition of the data at fracture. All data were continuously stored on magnetic media for immediate retrieval and post-processing. After failure, the fracture surface was coated with a light oil to preserve the fracture surface.

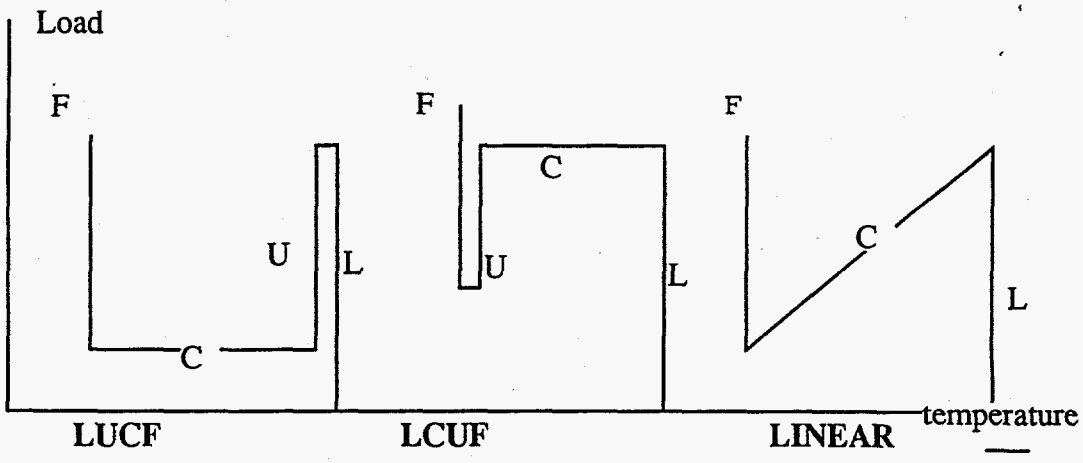

L = Load
C = Cool
F = Fracture
U = Unload

Figure A1. WPS Load/Temperature

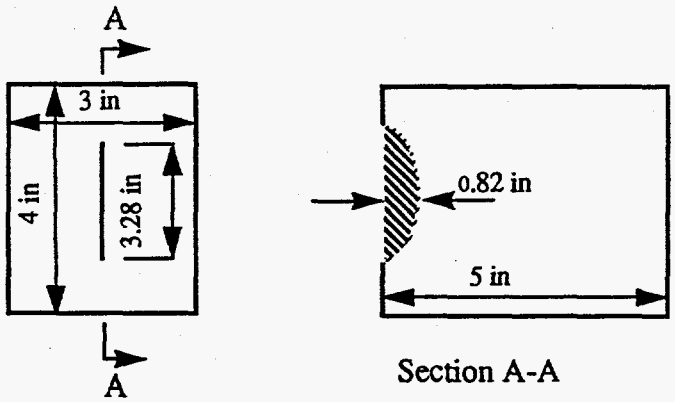

Figure A2. WPS Test Sections

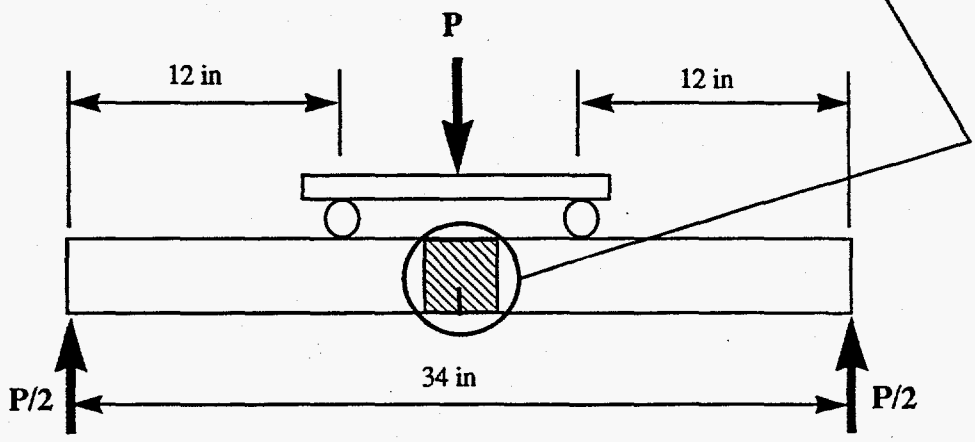

Figure A3. Schematic of WPS Test